Crystal Structure and Magnetism of the Double Perovskite $Sr_3Fe_2MoO_9$: A Neutron Diffraction Study

María C. Viola,[a] José A. Alonso,*[b] José C. Pedregosa,[a] and Raul E. Carbonio[c]

Keywords: Double perovskite / Neutron diffraction / Antiferromagnetic ordering

The $Sr_3Fe_2MoO_9$ double perovskite has been prepared in polycrystalline form by heat treatment, in air, from previously decomposed citrate precursors. This material has been studied by X-ray (XRD), neutron powder diffraction (NPD) and magnetic measurements. At room temperature, the crystal structure is tetragonal, space group *I*4/*m*, with $a = b = 5.5608(2)$ Å, $c = 7.8471(4)$ Å. It is convenient to write the crystallographic formula as $Sr_2Fe(Fe_{1/3}Mo_{2/3})O_6$, according to the usual nomenclature for double perovskites $A_2B'B''O_6$. The structure contains alternating FeO_6 and $(Fe,Mo)O_6$ octahedra, tilted by 3.9° in the basal *ab* plane. Magnetic measurements indicate a weak ferromagnetic behavior below $T_C = 280$ K. Ideally, the $Sr_3Fe_2MoO_9$ double perovskite only contains Fe^{3+} and Mo^{6+} cations, in such a way that superexchange interactions between neighboring Fe^{3+} spins are the only nominal mechanism accounting for the magnetism of this material. Our main finding is that this intrinsically "disordered" sample, containing a random distribution of Fe and Mo at the B′′ positions, exhibits a strong magnetic scattering on the low-angle Bragg positions, originating from naturally occurring groups of Fe^{3+} cations in which strong antiferromagnetic (AFM) Fe–O–Fe superexchange interactions are promoted, similar to those existing in the $LaFeO_3$ perovskite.

Introduction

In the search for new colossal magnetoresistant materials, some members of the family of double perovskites of composition $A_2B'B''O_6$ (A = alkaline earths; B′, B′′ = transition metals) have been proposed as half-metallic ferromagnets (best described as ferrimagnets), with T_C values well above room temperature, as an alternative to perovskite manganites.[1–5] The revival of interest in this family was triggered by a report on Sr_2FeMoO_6,[1] demonstrating that in the electronic structure only minority spins are present at the Fermi level: this material was shown to exhibit intrinsic tunnelling-type magnetoresistance (TMR) at room temperature.

TMR has also been described for double perovskites containing transition metals other than Mo, such as A_2FeReO_6 (A = Ca, Sr, Ba), which present a half-metallic ground state concomitant with the ferrimagnetic coupling of Fe^{3+} and Re^{5+} ($5d^2$, $S = 2/2$) magnetic moments, and show MR at room temperature. Also, Fe can be replaced by Co, as we have recently shown in Sr_2CoMoO_6,[6] where CMR properties were induced upon chemical reduction, by topotactical removal of oxygen atoms. Both examples illustrate the appealing possibility of searching for new CMR materials within the large family of double perovskite oxides.

The family of materials of the type $A_3B'_2B''O_9$ (A = Ca, Sr, Ba; B′ = transition metal and B′′ = Mo, W, Te or U) has recently attracted our attention. These compounds are also double perovskites whose crystallographic formula could be re-written as $A_2B'(B'_{1/3}B''_{2/3})O_6$. They, thus, display an intrinsic partial disordering over half of the perovskite ($B'_{1/3}B''_{2/3}$) positions. We have prepared different materials with A = Ca, Sr; B′ = Fe and B′′ = Mo, W, Te or U and with X-ray diffraction and Mössbauer spectroscopy we have shown that all the compounds are tetragonal and can be refined in the space group *I*4/*m*.[7] This is the same symmetry and space group found for Sr_2FeMoO_6 or Sr_2CoMoO_6. Additionally, an increase in the disorder of B′′ among the Wyckoff sites 2*a* and 2*b* in the sequence Mo < U < Te < W was found. This degree of disorder is observed as an increase in the width of the Mössbauer lines.[7] The sextuplet displayed in the Mössbauer spectra implies a room-temperature magnetic order for B′′ = U, Te and W. For B′′ = Mo two iron sites are observed as two different doublets, indicative of iron occupying the two different positions (2*a* and 2*b*).

These data have now been complemented with microscopic neutron powder diffraction (NPD) data on $Sr_3Fe_2MoO_9$. In this paper we report on the results of a

[a] Area de Química General e Inorgánica "Dr. Gabino F. Puelles", Departamento de Química, Facultad de Química, Bioquímica y Farmacia, Universidad Nacional de San Luis, Chacabuco y Pedernera, 5700 San Luis, Argentina
[b] Instituto de Ciencia de Materiales de Madrid, C.S.I.C., Cantoblanco, 28049 Madrid, Spain
[c] Instituto de Investigaciones en Físico Química de Córdoba (INFIQC), Departamento de Fisicoquímica, Facultad de Ciencias Químicas, Universidad Nacional de Córdoba, Ciudad Universitaria, 5000 Córdoba, Argentina

high-resolution NPD study, giving a detailed description of the crystal structure as well as its thermal evolution down to 2 K. This study also gives insight on the magnetic structure of this material, which shows an intrinsically high magnetic disordering over the B′′ = Fe/Mo positions. Macroscopic magnetic measurements are also reported and discussed. We show that, in spite of small saturation magnetization exhibited by $Sr_3Fe_2MoO_9$, the magnetic neutron scattering is surprisingly strong for such a magnetically disordered sample. We ascribe the observed scattering to Fe-rich regions, where strong Fe–O–Fe superexchange interactions give rise to the antiferromagnetic (AFM) ordering of the neighboring Fe spins.

Results

$Sr_3Fe_2MoO_9$ was obtained as a black, well-crystallized powder. The XRD pattern is characteristic of a perovskite structure, showing the splitting of certain reflections, characteristic of a tetragonal distortion [for instance, (004) and (220) reflections]. Minor amounts of $SrMoO_4$ were detected from either XRD or NPD data.

Magnetic Data

The magnetic susceptibility vs. temperature curves are displayed in Figure 1. Below 280 K the zero-field-cooled (ZFC) and field-cooled (FC) curves exhibit a distinct evolution. The FC curve shows a progressive increment of the susceptibility as temperature decreases, reminiscent of the spontaneous evolution characteristic of a ferromagnet, although a very small saturation magnetization is reached at low temperatures, of only 0.004 μ_B/f.u. with a measuring field of H = 1000 Oe. The ZFC curve shows a less pronounced susceptibility increment as temperature decreases, and exhibits a broad maximum increment centered at 60 K, suggesting the establishment of a long-range AFM ordering below this temperature. The magnetization vs. magnetic field curves at 2, 100, and 300 K are plotted in Figure 2. Even at the lowest temperature, the magnetization is very far from saturation for the maximum applied field of H = 3 T, reaching a maximum value of 0.15 μ_B/f.u. The hysteretic behavior is characteristic of a weak ferromagnetic system.

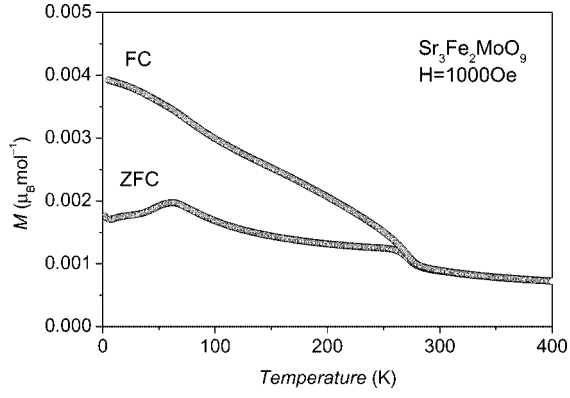

Figure 1. Field-cooled (FC) and zero-field-cooled (ZFC) magnetic susceptibility vs. temperature curves for $Sr_3Fe_2MoO_9$.

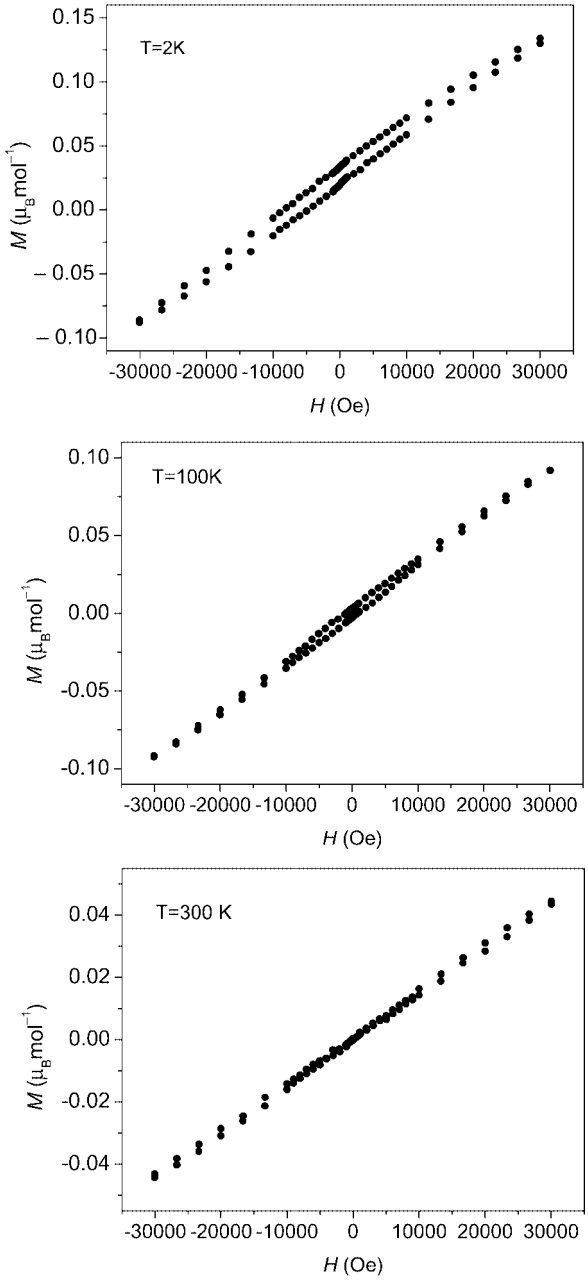

Figure 2. Magnetization vs. magnetic field isotherms (T = 2, 100, and 300 K) for $Sr_3Fe_2MoO_9$.

Structural Refinement

The structural refinement of $Sr_3Fe_2MoO_9$ from room-temperature high-resolution NPD data was performed in the *I*4/*m* space group (No. 87), with unit-cell parameters related to a_0 (ideal cubic perovskite, a_0 = 3.9 Å) as $a = b \approx 2^{1/2} \cdot a_0$ and $c \approx 2a_0$. Sr atoms were located at 4*d* (0,1/2,1/4) positions, Fe/Mo at 2*a* (0,0,0) and Fe at 2*b*(0,0,1/2) sites, and oxygen atoms at 4*e* (0,0,*z*) and 8*h* (*x*,*y*,*z*) positions.

$SrMoO_4$ was included in the refinement as a second phase, defined[8] in the space group $I4_1/a$ (10.87% of this phase from the scale factors). No *anti*-site disordering was detected, by assuming that some Mo from the 2*a* positions could randomly replace some Fe at the 2*b* positions. In the final refinement, the Fe/Mo occupancy over the 2*a* positions was also allowed to change from the nominal Fe/Mo = 2:1 stoichiometry; no departure from this nominal occupancy was detected within the standard deviations (Table 1). An excellent agreement between observed and calculated NPD profiles was obtained for this model, as illustrated in Figure 3. Table 1 includes the final atomic coordinates and discrepancy factors after the refinement. Table 2 lists the main interatomic distances and angles. A drawing of the structure is shown in Figure 4. The structure contains alternating FeO_6 and $(Fe,Mo)O_6$ octahedra, tilted in *anti*-phase in the basal *ab* plane (along the [001] direction of the pseudocubic cell). This corresponds to the $a^0a^0c^-$ Glazer's notation as derived by Woodward[9] for 1:1 ordering of double perovskites, consistent with space group *I*4/*m*.

Table 1. Positional and thermal parameters for $Sr_2Fe(Fe_{1/3}Mo_{2/3})O_6$ after the Rietveld refinement[a] from NPD data taken at 298 K, space group: *I*4/*m*, $Z = 2$. Unit-cell parameters: $a = b = 5.5608(2)$ Å, $c = 7.8471(4)$ Å, $V = 242.65(2)$ Å^3.

Atom	Wyckoff site	*x*	*y*	*z*	B_{iso} [Å^2]	Occ.
Sr	4*d*	0.0000	0.5000	0.0000	0.97(2)	1.00
Fe	2*a*	0.0000	0.0000	0.0000	0.1(2)	0.33(3)
Mo	2*a*	0.0000	0.0000	0.0000	0.1(2)	0.66(3)
Fe	2*b*	0.0000	0.0000	0.5000	0.9(2)	1.00
O1	4*e*	0.0000	0.0000	0.247(5)	1.3(1)	1.00
O2	8*h*	0.269(3)	0.235(3)	0.0000	1.13(6)	1.00

[a] Discrepancy factors: $R_{Bragg} = 3.48\%$, $R_{wp} = 13.7\%$, $R_{exp} = 4.78\%$, $\chi^2 = 8.21$.

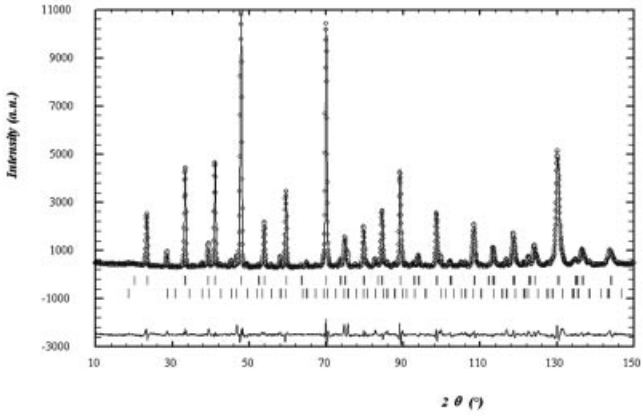

Figure 3. Observed (open circles), calculated (full line) and difference (bottom) NPD Rietveld profiles for $Sr_3Fe_2MoO_9$ at 295 K. The second series of tick marks corresponds to the Bragg reflections of the $SrMoO_4$ impurity phase.

Magnetic Structure

The sequential data collection at D20 from 2 to 262 K showed a strong magnetic contribution to the scattering on

Table 2. Some selected bond lengths [Å] and angles [°] for $Sr_2Fe(Fe_{1/3}Mo_{2/3})O_6$.

Distances	
SrO_{12} icosahedron	
(Sr)–(O1)(x4)	2.7805(4)
(Sr)–(O2)(x4)	2.87(1)
(Sr)–(O2)(x4)	2.69(1)
⟨Sr–O2⟩	2.780(5)
$(Fe/Mo)_{2a}O_6$ octahedron	
$(Fe/Mo)_{2a}$–(O1)(x2)	1.93(4)
$(Fe/Mo)_{2a}$–(O2)(x4)	1.99(2)
$\langle(Fe)_{2b}–O\rangle$	1.97(3)
$Fe_{2b}O_6$ octahedron	
$(Fe)_{2b}$–(O1)(x2)	1.99(2)
$(Fe)_{2b}$–(O2)(x4)	1.93(4)
$\langle(Fe)_{2b}–O\rangle$	1.97(3)
Angles	
$(Fe)_{2b}$–(O1)–$(Fe/Mo)_{2a}$	180.00
$(Fe)_{2b}$–(O2)–$(Fe/Mo)_{2a}$	172.3(6)

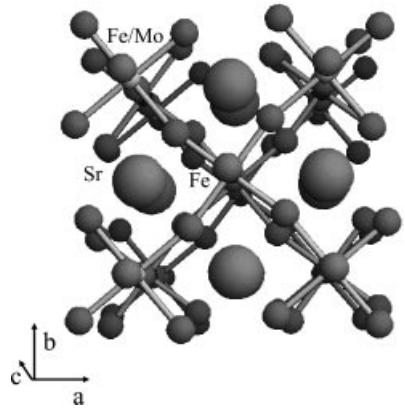

Figure 4. View of the structure of tetragonal $Sr_2Fe(Fe_{1/3}Mo_{2/3})O_6$ approximately along the *c* axis. Large spheres represent Sr; corner-sharing FeO_6 (dark) and $(Fe,Mo)O_6$ octahedra are tilted in *anti*-phase along the *c* axis, in order to optimize Sr–O bond lengths.

allowed Bragg positions ($k = 0$), mainly on the (011) reflection (Figure 5), suggesting a ferro- or ferrimagnetic long-range ordering. This is surprising in this strongly disordered sample, taking into account that the saturation magnetization is very small, of hardly 0.15 μ_B/f.u. with an applied field of 3 T. We would have expected that the structural disordering at the B positions of the perovskite had led to the absence of long-range magnetic ordering between Fe and Mo magnetic moments. As it will be discussed later, we believe that this magnetic scattering originates from Fe-rich patches in which neighboring Fe^{3+} spins exhibit AFM superexchange interactions via Fe–O–Fe paths. We have thus modeled the magnetic structure as a perfect AFM arrangement of Fe spins with alternating directions, occupying all the B positions of a perovskite structure with the same unit-cell and positional parameters as the host $Sr_3Fe_2MoO_9$ perovskite. We have constrained the scale factors of both structural and magnetic models, and refined the magnitude of the Fe magnetic moments. The goodness of the fit is shown in Figure 6, where both structural and magnetic contributions to the scattering have been in-

cluded. The thermal variation of the magnitude of the ordered Fe magnetic moments is displayed in Figure 7.

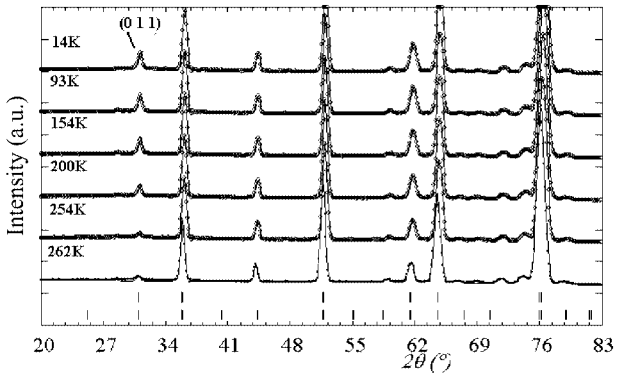

Figure 5. Thermal evolution of the NPD patterns dynamically collected with the high-flux D20 diffractometer, highlighting the appearance at low temperatures of a magnetic contribution to the scattering on the low-angle reflections, especially on the (011) Bragg position.

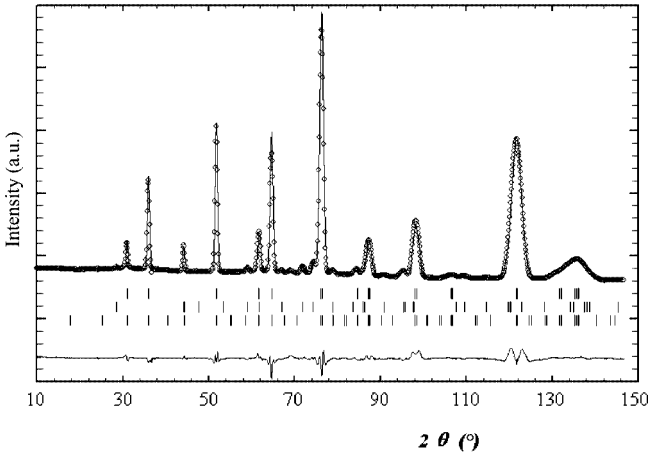

Figure 6. Observed (open circles) and calculated (full line) NPD profiles at 2 K. The three series of allowed Bragg reflections correspond to the crystallographic phase, the $SrMoO_4$ impurity and the magnetic structure for the AFM model described in the text. Unit-cell parameters are $a = b = 5.5346$, $c = 7.8553$ Å; discrepancy factors: $R_{wp} = 3.03\%$, $R_{bragg} = 4.49\%$; $R_{mag} = 11.4\%$.

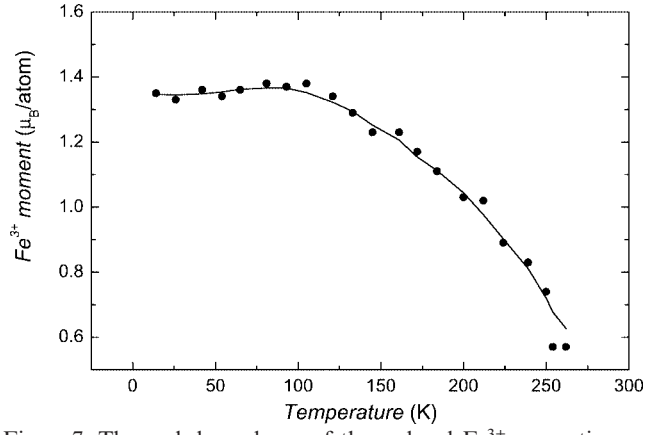

Figure 7. Thermal dependence of the ordered Fe^{3+} magnetic moments sequentially refined from D20 NPD data.

Discussion

Recently, Woodward[9] has described the possible tilting systems for $A_2B'B''O_6$ ordered perovskites, predicting the space groups for each system. When the A cation is large enough, the well-known $(NH_4)_3FeF_6$ structure is adopted by the 1:1 B-site ordered perovskites, such as Ba_2FeMoO_6, which can be described in the cubic space group $Fm\bar{3}m$. For slightly smaller A cations, only a small deformation of the lattice takes place, implying the tilting of the octahedra only along the *c* axis. This tilting means a reduction in symmetry from cubic to tetragonal. The structure of $Sr_3Fe_2MoO_9$, which can ideally be rewritten as $Sr_2Fe(Fe_{1/3}Mo_{2/3})O_6$, is defined in the space group *I*4/*m*, and can be described as the result of a single *anti*-phase octahedral tilting along the *c* axis. Figure 4 illustrates this particular feature. A tilting of 3.9° at room temperature can be derived from the B′–O2–B′′ angle.

The refinement of the occupancy factors of Fe and Mo over the B′′ sites from NPD data indicates a Fe/Mo = 2:1 ratio (within the standard deviations), and no *anti*-site disordering effect was detected, excluding the possibility that some Mo cations could partially replace Fe cations at the 2*b* positions; the actual crystallographic formula is $Sr_2(Fe)_{2b}(Fe_{0.33(3)}Mo_{0.67(3)})_{2a}O_6$. In contrast with Sr_2FeMoO_6, which must be prepared under reducing conditions in order to provide a mixed valence Fe^{3+}–Fe^{2+}/Mo^{5+}–Mo^{6+} state, the present $Sr_3Fe_2MoO_9$ perovskite has been synthesized in air, in such a way that, from the chemical point of view, we should assign a nominal hexavalent oxidation state to the Mo cations, making all Fe cations nominally trivalent. From this point of view, the electronic configuration for this sample would be $Fe^{3+}(3d^5)$–$Mo^{6+}(4d^0)$.

On reinvestigating the example of Sr_2FeMoO_6, electronic band calculations show that the up-spin band, placed below the Fermi level, is mainly occupied by five Fe 3d electrons forming localized spins on the Fe sites. The down-spin band, which has density of states at the Fermi level, is composed mainly of hybridized Mo 4d t_{2g} and Fe 3d t_{2g} states. Thus, the Mo electron which occupies the down-spin band is itinerant and it is shared among Fe and Mo sites.[10–12] The high degree of itinerancy of the Mo electron is responsible for the high conductivity; the superexchange interaction between the localized Fe moment and the partially localized Mo moment accounts for the ferrimagnetic behavior of Sr_2FeMoO_6. Ideally, a perfectly ordered Sr_2FeMoO_6 perovskite should exhibit a saturation magnetization of 4 μ_B/f.u.; in reality, 3.6–3.8 μ_B/f.u. values are obtained due to *anti*-site disordering effects.[13]

In the present $Sr_3Fe_2MoO_9$ material, nominally containing only Fe^{3+} and Mo^{6+}, the lack of an itinerant Mo electron would prevent the magnetic coupling across Fe–O–Mo paths, in such a way that the only possible magnetic superexchange mechanism would take place via Fe–O–Fe paths, in Fe-rich areas of the crystal containing neighboring Fe^{3+} spins. Figure 8 shows a simplified image of the magnetic ordering in this disordered sample; only one layer of B cations is shown for the sake of simplicity. A perfect ferrimag-

netic coupling between up Fe^{3+} spins at 2*b* sites (black in Figure 8) and down Fe^{3+} spins at 2*a* positions (grey in Figure 8) would ideally give $5\cdot(1 - 1/3) = 2.66\ \mu_B$/f.u., but this would require perfect coherence between Fe-rich patches, as illustrated in Figure 8. Notice that the total absence of coherence between isolated Fe-rich patches would lead, on average, to a null saturation magnetization. In fact, in contrast with Sr_2FeMoO_6, in the double perovskite $Sr_3Fe_2MoO_9$ we observe a strong suppression of the global FM properties although there is a remanent weak FM effect which corresponds to the statistical coherence: for a cubic lattice where B′ = Fe and B′′ is statistically occupied by 1/3 Fe, the long-range magnetic connections through B′–B′′(Fe)–B′ exceed the 31% percolation limit of a simple cubic lattice. The tetragonal distortion observed here does not change these considerations. Only $(2/3)^6 = 9\%$ of the B′ site Fe atoms are not connected to at least one B′′ site Fe^{3+}; these nonconnected atoms are labeled as "?" in Figure 8.

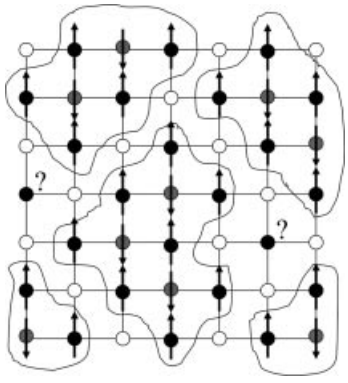

Figure 8. Ideal schematic view of the magnetic coupling in $Sr_2Fe(Fe_{1/3}Mo_{2/3})O_6$. This double perovskite contains Fe at 2*b* positions (black atoms and spins) and randomly distributed Fe (grey atoms and spins) and Mo (white atoms) at 2*a* positions. AFM magnetic coupling is via Fe–O–Fe paths (along the lines). Naturally occurring Fe-rich patches are antiferromagnetically coupled, and there is magnetic coherence between some adjacent patches.

One of the main issues to be addressed in this paper is the origin of the magnetic scattering on the sample showing an important component of intrinsic Fe/Mo disordering. We have been able to accurately fit the magnetic contributions to the neutron scattering by modeling an AFM structure consisting of a perfect arrangement of Fe cations occupying all of the B positions of a perovskite structure with the same unit-cell parameters as the crystallographic $Sr_3Fe_2MoO_9$ phase. The refinement of the magnitude of the magnetic moments on the Fe positions, at 2 K, gives an ordered magnetic moment of 1.4 μ_B, with constrained scale factors for the crystal and magnetic structure. Notice that this is only the average ordered component of the magnetic moment over all the B positions of the perovskite. Our picture thus shows a disordered Fe/Mo pattern in which the Fe–O–Fe superexchange AFM interactions are comparable to those existing in $RFeO_3$ ferrites (R = rare earths). As illustrated in Figure 8, the coupling between near-neighbor Fe–O–Fe cations is always AFM; the important fact is that the coherence between the magnetic ordering of isolated Fe–O–Fe patches is statistically maintained across the solid; the long-range coherence is naturally weaker than that corresponding to a completely ordered compound. Only below temperatures around 30–60 K would the super-superexchange mechanism across Fe–O–Mo–O–Fe paths trigger a complete long-range AFM ordering, as it happens in the antiferromagnet Sr_2FeWO_6 below $T_N = 37$ K.[14] Moreover, we could assign the maximum observed in the ZFC susceptibility curve at 60 K to the onset of these super-superexchange interactions, in addition to the interactions coming from the statistical connections between Fe-rich patches. The thermal variation of the magnetic moment on Fe positions (Figure 7) exhibits an abrupt decay at 250 K, which corresponds to the vanishing of the long-range antiferromagnetic ordering of Fe^{3+} spins, in agreement with the magnetic susceptibility curve.

Conclusions

$Sr_3Fe_2MoO_9$ perovskite is a weak ferromagnet by virtue of the partial long-range coherence established between antiferromagnetically ordered patches of Fe^{3+} spins, composed by some tenths of atoms, naturally arising from the statistical disordering exhibited by this material. The crystal structure, refined from NPD data in the *I*4/*m* space group, contains two kinds of B positions; one of them is fully occupied by Fe^{3+} cations whereas the second one contains a random distribution of Fe^{3+} and Mo^{6+} cations. Below 280 K, the superexchange Fe–O–Fe interactions within naturally occurring Fe-rich patches account for the observed magnetic behavior and the appearance of a significant contribution to the magnetic scattering on the low-angle Bragg reflections. The coherence between isolated Fe-rich patches is statistically provided; only 9% of Fe atoms are magnetically isolated. At lower temperatures, around 60 K, super-superexchange Fe–O–Mo–O–Fe interactions contribute to the long-range AFM ordering of the majority of Fe^{3+} spins. The thermal variation of the ordered Fe^{3+} magnetic moments shows an abrupt decay above 250 K, in agreement with the macroscopic magnetic properties.

Experimental Section

The $Sr_3Fe_2MoO_9$ perovskite was prepared as a black polycrystalline powder from citrate precursors obtained by soft chemistry procedures. Stoichiometric amounts of analytical grade $Sr(NO_3)_2$, $Fe(C_2O_4)\cdot 2H_2O$, and $(NH_4)_6Mo_7O_{24}\cdot 4H_2O$ were dissolved in citric acid. The citrate, nitrate and oxalate solutions were slowly concentrated, leading to organic resins containing a random distribution of the cations involved at an atomic level. These resins were first dried at 120 °C and then slowly decomposed at temperatures up to 600 °C. All the organic materials and nitrates were eliminated in a subsequent treatment at 800 °C in air, for 2 h. This treatment gave rise to highly reactive precursor materials. The resulting black powder was then treated in air at 1000 °C for 24 h and 1150 °C for 48 h.

The initial characterization of the product was carried out by laboratory X-ray diffraction (XRD) measurements (Cu-K_α, λ =

1.5418 Å). For the structural refinements, a room-temperature NPD pattern was collected with the high-resolution D2B neutron diffractometer (ILL-Grenoble, France). The high-flux mode was used. About 4 g of sample was contained in a vanadium can; the counting time was 3 h. A wavelength of 1.594 Å was selected from a Ge monochromator. The variable-temperature NPD patterns in the range 2–262 K were collected at the D20 high-flux neutron diffractometer (ILL, Grenoble, France), using a wavelength of 2.42 Å, in order to obtain information about the low-temperature magnetic structure and its thermal variation. A standard cryostat was used for the sequential collections. A collimation of 27" was selected. Once cooled to 2 K, the sample was heated at 2 K min^{-1} and the NPD patterns were sequentially collected with counting times of 2 min.

All the patterns were refined by the Rietveld method by using the FULLPROF refinement program.[15] A pseudo-Voigt function was chosen to generate the line shape of the diffraction peaks. The minor $SrMoO_4$ impurity (with scheelite structure) was included as a second crystallographic phase in the refinements. In the final runs, the following parameters were refined: scale factors for the main and impurity phases, background coefficients, zero-point error, unit-cell parameters, pseudo-Voigt corrected for asymmetry parameters, positional coordinates, isotropic thermal factors, *anti*-site disorder for Fe/Mo and occupancy factors for oxygen atoms. The coherent scattering lengths for Sr, Fe, Mo, and O were 7.02, 9.45, 6.72, and 5.803 fm, respectively.

Acknowledgments

We acknowledge the financial support of CICyT for the project MAT2004-0479 and we are grateful to ILL for making all facilities available. J. C. P., M. C. V. and R. E. C. acknowledge the financial support of the Consejo Nacional de Investigaciones Científicas y Técnicas (CONICET PID 4929/96, PIP 380/98 and PIP 02482), the Agencia Nacional de Promoción Científica y Tecnológica (PICT98 06-03041 and PICT99 12-5378), Fundación Antorchas (collaboration project A-13740/1-94), CyT (Universidad Nacional de San Luis – Project 7707) and SECyT-UNC. J. C. P. and R. E. C. are members of CONICET. We acknowledge financial support provided by a CSIC-CONICET collaboration project.

[1] K.-I. Kobayashi, T. Kimura, H. Sawada, K. Terakura, Y. Tokura, *Nature* **1998**, *395*, 677.
[2] B. García-Landa, C. Ritter, M. R. Ibarra, J. Blasco, P. A. Algarabel, R. Mahendiran, J. García, *Solid State Commun.* **1999**, *110*, 435.
[3] A. Maignan, B. Raveau, C. Martin, M. Hervieu, *J. Solid State Chem.* **1999**, *144*, 224.
[4] K.-I. Kobayashi, T. Kimura, Y. Tomioka, H. Sawada, K. Terakura, Y. Tokura, *Phys. Rev. B* **1999**, *59*, 11159.
[5] T. H. Kim, M. Uehara, S.-W. Cheong, S. Lee, *Appl. Phys. Lett.* **1999**, *74*, 1737.
[6] M. C. Viola, M. J. Martínez-Lope, J. A. Alonso, P. Velasco, J. L. Martínez, J. C. Pedregosa, R. E. Carbonio, M. T. Fernández-Díaz, *Chem. Mater.* **2002**, *14*, 812.
[7] M. C. Viola, M. S. Ausburger, R. M. Pinnaca, J. C. Pedregosa, R. E. Carbonio, R. C. Mercader, *J. Solid State Chem.* **2003**, *175*, 252.
[8] E. Guermen, E. Daniels, J. S. King, *J. Chem. Phys.* **1971**, *55*, 1093.
[9] P. M. Woodward, *Acta Crystallogr., Sect. B* **1997**, *53*, 32.
[10] O. Chmaissem, R. Kruk, B. Dabrowski, D. E. Brown, X. Xiong, S. Kolesnik, J. D. Jorgensen, C. W. Kimball, *Phys. Rev. B* **2000**, *62*, 14197.
[11] D. D. Sarma, E. V. Sampathkumaran, S. Ray, R. Nagarajan, S. Majumdar, A. Kumar, G. Nalini, T. N. Guru Row, *Solid State Commun.* **2000**, *114*, 465.
[12] A. S. Ogale, S. B. Ogale, R. Ramesh, T. Venkatessan, *Appl. Phys. Lett.* **1999**, *75*, 537.
[13] Ll. Balcells, J. Navarro, M. Bibes, A. Roig, B. Martínez, J. Fontcuberta, *Appl. Phys. Lett.* **2001**, *78*, 781.
[14] A. K. Azad, S.-G. Eriksson, A. Mellergard, S. A. Ivanov, J. Eriksen, H. Rundlöf, *Mater. Res. Bull.* **2002**, *37*, 1797.
[15] J. Rodríguez-Carvajal, *Physica B (Amsterdam)* **1993**, *192*, 55.
Received: September 8, 2004

